

Fig. 2 Body weight curve of rats treated with zinc oxide in the 13-week intratracheal repeated dose test. A significant inhibition in the normal increase of body weight was observed at the highest dose of 2 mg/kg.

153.5, 1.25, and 12.0  $\mu\text{g/ml}$  (Fig. 1), respectively, in the cytotoxicity test. Only zinc oxide induced structural CAs (Table 1).

In the 13-week repeated dose test, the normal increase in mean body weight was significantly inhibited at 2 mg/kg of zinc oxide (Fig. 2), although no clinical signs were found in rats treated with all test suspensions.

Histopathologically, granulomatous inflammation with foamy cells in the alveoli or surrounding the bronchiole and perivascular cell infiltration were detected as common lesions in rats treated with three test suspensions. The lesions increased in their intensities with dose, and similarly distributed in all the lobes indicating that they were evenly exposed to the NMs.

On the other hand, alveolar epithelial hyperplasia was prominent in rats treated with silver than with silica.

Microgranuloma and aggregation of foamy cells were found in the mediastinal lymph node at higher doses of silica and silver, indicating that macrophages with NMs phagocytosed moved to lymph node through lymphatic vessels. Zinc oxide markedly induced proliferation of alveolar/bronchial epithelium and mucinous cells in bronchus and fibrosis at two highest doses. NOEL of silica, silver, and zinc oxide was less than 0.06, 0.004, and less than 0.0312 mg/kg, respectively.

## Conclusions

The three tests performed in the present study showed characteristic results of

each nano-suspension. It suggests that they may be a set of useful tools to screen NMs for safety evaluation, although further studies are needed to confirm the fact.

### References

1. MATSUOKA A. *et al.*, Development of an *in vitro* screening method for safety evaluation of nanomaterials, *Biomed. Mater. Eng.* 19, 19-27 (2009)

### Acknowledgement

This study was partially supported by the Health and Labour Sciences Research Grants (H22-IYAKU-IPPAN-009).

# Chiral analyses of dextromethorphan/levomethorphan and their metabolites in rat and human samples using LC-MS/MS

Ruri Kikura-Hanajiri · Maiko Kawamura ·  
Atsuko Miyajima · Momoko Sunouchi · Yukihiro Goda

Received: 30 September 2010 / Revised: 7 January 2011 / Accepted: 22 January 2011  
© Springer-Verlag 2011

**Abstract** In order to develop an analytical method for the discrimination of dextromethorphan (an antitussive medicine) from its enantiomer, levomethorphan (a narcotic) in biological samples, chiral analyses of these drugs and their *O*-demethyl and/or *N*-demethyl metabolites in rat plasma, urine, and hair were carried out using LC-MS/MS. After the i.p. administration of dextromethorphan or levomethorphan to pigmented hairy male DA rats (5 mg/kg/day, 10 days), the parent compounds and their three metabolites in plasma, urine and hair were determined using LC-MS/MS. Complete chiral separation was achieved in 12 min on a Chiral CD-Ph column in 0.1% formic acid–acetonitrile by a linear gradient program. Most of the metabolites were detected as being the corresponding *O*-demethyl and *N*, *O*-didemethyl metabolites in the rat plasma and urine after the hydrolysis of *O*-glucuronides, although obvious differences in the amounts of these metabolites were found between the dextro and levo forms. No racemation was observed

through *O*- and/or *N*-demethylation. In the rat hair samples collected 4 weeks after the first administration, those differences were more clearly detected and the concentrations of the parent compounds, their *O*-demethyl, *N*-demethyl, and *N*, *O*-didemethyl metabolites were 63.4, 2.7, 25.1, and 0.7 ng/mg for the dextro forms and 24.5, 24.6, 2.6, and 0.5 ng/mg for the levo forms, respectively. In order to fully investigate the differences of their metabolic properties between dextromethorphan and levomethorphan, DA rat and human liver microsomes were studied. The results suggested that there might be an enantioselective metabolism of levomethorphan, especially with regard to the *O*-demethylation, not only in DA rat but human liver microsomes as well. The proposed chiral analyses might be applied to human samples and could be useful for discriminating dextromethorphan use from levomethorphan use in the field of forensic toxicology, although further studies should be carried out using authentic human samples.

Published in the special issue *Forensic Toxicology* with Guest Editors Frank T. Peters, Hans H. Maurer, and Frank Musshoff.

R. Kikura-Hanajiri (✉) · M. Kawamura · Y. Goda  
Division of Pharmacognosy, Phytochemistry and Narcotics,  
National Institute of Health Sciences,  
1-18-1, Kamiyoga, Setagaya,  
Tokyo 158-8501, Japan  
e-mail: kikura@nihs.go.jp

A. Miyajima  
Division of Medical Devices,  
National Institute of Health Sciences,  
1-18-1, Kamiyoga, Setagaya,  
Tokyo 158-8501, Japan

M. Sunouchi  
Division of Pharmacology, National Institute of Health Sciences,  
1-18-1, Kamiyoga, Setagaya,  
Tokyo 158-8501, Japan

**Keywords** Levomethorphan · Dextromethorphan · Chiral analysis · Biological samples · LC-MS/MS · Enantioselective metabolism

## Introduction

Dextromethorphan is widely used all over the world as an over-the-counter antitussive medicine. It produces little or no central nervous system depression at therapeutic doses, but it has dissociative effects similar to ketamine and phencyclidine in large doses as an *N*-methyl-*D*-aspartate receptor antagonist [1–6]. To obtain its hallucinogenic effect, young people abuse this drug by large doses and many fatalities from overdoses have been reported [7, 8]. In

contrast, its enantiomer, levomethorphan, is a potent narcotic analgesic [9] (Fig. 1), and an *O*-demethyl compound of levomethorphan, levorphanol, is known to have stronger opioid pharmacological effects [9, 10]. Levomethorphan is strictly controlled in the world as a narcotic and is never used for therapeutic purposes.

In humans, as shown in Fig. 2, it has been reported that dextromethorphan is primarily metabolized to dextrorphan via *O*-demethylation by cytochrome P450 2D6 (CYP2D6), which is polymorphically expressed in humans, who can be classified as poor, intermediate, and extensive metabolizers [11, 12]. Dextromethorphan is *N*-demethylated via an additional route to 3-methoxymorphinan (3-MEM), primarily mediated by CYP3A4 in human liver microsomes [11, 13]. Dextrorphan and 3-MEM are then demethylated to 3-hydroxymorphinan (3-HM) via CYP3A4 and CYP2D6, respectively. Moreover, dextrorphan and 3-HM are glucuronized to their *O*-glucuronides and these are mainly excreted into human urine [14, 15].

A variety of analytical methods for the determination of dextromethorphan and its metabolites in biological samples have been reported using capillary electrophoresis (CE) [16, 17], HPLC [18–22], GC-MS [23–26], and LC-MS (/MS) [15, 27–30]. However, there is little information regarding the metabolic properties of levomethorphan. Although a chiral separation method of dextromethorphan and levomethorphan using HPLC with fluorometric detection [22] or using CE [17] has been reported, there has been no report that describes a simultaneous determination of dextromethorphan, levomethorphan, and their metabolites in biological samples after administration of these drugs. Considering the possibility of the adulteration or substitution of dextromethorphan with levomethorphan due to its chemical similarities for illegal purposes, it is necessary to establish the enantiometric separation of dextromethorphan and levomethorphan in biological samples.

In order to develop an analytical method for the discrimination of dextromethorphan from levomethorphan in biological samples, we first investigated chiral analyses of these drugs and their *O*-demethyl and/or *N*-demethyl metabolites in plasma, urine, and hair samples of rats administered with each enantiomer, using LC-MS/MS. In

addition, detailed metabolic properties of these drugs were investigated using rat and human liver microsomes.

## Experimental

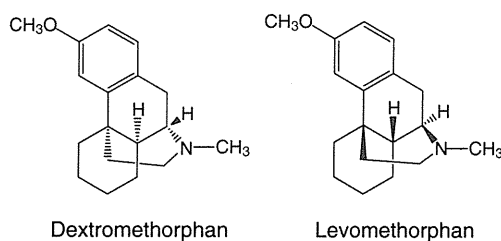
### Materials

Levomethorphan was obtained from Cerilliant (Round Rock, TX, USA). Dextromethorphan hydrobromide, dextrorphan tartrate, (+)-3-HM hydrobromide, (+)-3-MEM hydrochloride, and levallorphan tartrate (used as internal standard, IS) were from Sigma-Aldrich (St. Louis, MO, USA). Levorphanol tartrate was given by Professor T. Nagano (Graduate School of Pharmaceutical Sciences, The University of Tokyo, Japan). A  $\beta$ -glucuronidase solution (EC 3.2.1.31, 103,000 units/mL, Source: *Helix pomatia*) was purchased from Wako Chemicals (Osaka, Japan). A solid-phase extraction column (OASIS HLB, 3 cc, 60 mg) was obtained from Waters (Milford, MA, USA), and the membrane filter (Ultrafree-MC, 0.45  $\mu$ m) was from Millipore Corporation (Bedford, MA, USA).

Liver microsomes from individual male dark agouti (DA) rats ( $n=4$ , 6 weeks old, around 125 g mean weight) were prepared by ultracentrifugation as described [31, 32]. The concentrations of microsomal protein were estimated using a bicinchoninic acid (BCA) protein assay kit (Pierce, Rockford, IL). Human liver microsomes (50-donor pool, 20 mg/mL) were purchased from BD Biosciences (Woburn, MA, USA). Nicotinamide adenine dinucleotide phosphate (NADP) and glucose 6-phosphate (G-6-P) were obtained from Oriental Yeast Co., Ltd. (Tokyo, Japan) and G-6-P dehydrogenase (G-6-PDH) was from Roche Diagnostics (Indianapolis, IN, USA). All other chemicals and solvents were of an analytical reagent grade or HPLC grade (Wako Chemicals, Osaka, Japan).

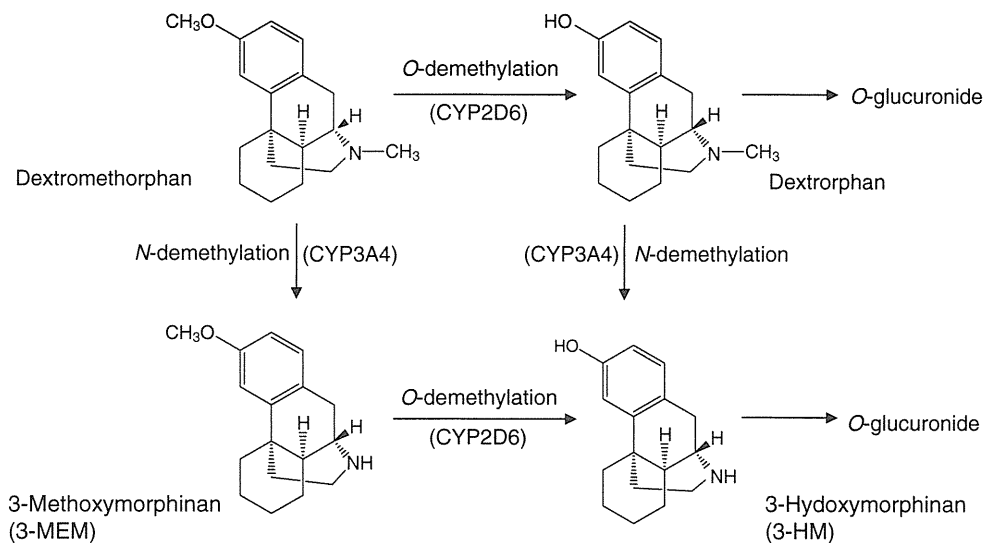
### Instrumentation

The UPLC analysis was performed using a Waters Acquity Ultra-Performance™ liquid chromatography system (Waters, Milford, MA, USA). The separations were achieved using a Chiral CD-Ph column (150×2.1 mm i.d., 5  $\mu$ m) from Shiseido (Tokyo, Japan). The column temperature was maintained at 30 °C, and the following gradient system was used with a mobile phase A (0.1% formic acid) and mobile phase B (0.1% formic acid/acetonitrile) delivered at 0.25 mL/min: 80% A/20% B (2 min hold)—70% A/30% B (15 min). The mobile phase was used as a wash solvent to avoid any carry-over from previous injections. The auto-sampler was maintained at 4 °C, and the injection volume was 2  $\mu$ L. Quantitation was achieved by MS/MS detection in a positive ion mode using a Quattro Premier XE mass



**Fig. 1** Chemical structures of dextromethorphan and its enantiomer, levomethorphan



**Fig. 2** Main metabolic pathway of dextromethorphan in humans

spectrometer (Waters, Milford, MA, USA) equipped with an electrospray ionization (ESI) interface. Quantification was performed using multiple reaction monitoring of the transitions of precursor ions to product ions with each cone voltage and collision energy as shown in Table 1. The optimal MS parameters obtained were as follows: capillary 3.0 kV, source temperature 120 °C, and desolvation temperature 350 °C. Nitrogen was used as the desolvation and cone gas, with a flow rate of 800 and 50 L/h, respectively. Argon was used as the collision gas, with a flow rate of 0.25 mL/min. All data collected in the centroid mode were processed using MassLynx™ NT4.1 software with a QuanLynx™ program (Waters, Milford, MA, USA).

Since the standard compounds of (–)-3-MEM and (–)-3-HM were not available, these peaks were confirmed by comparison of their retention times and mass fragmentations with those of the standard compounds of the dextro forms ((+)-3-MEM and (+)-3-HM) using an ODS column. The analyses were performed using an Acquity HSS T3 column (100×2.1 mm i.d., 1.8 μm) from Waters (Milford, MA, USA). The column temperature was maintained at 40 °C, and the following gradient system was used with a mobile phase A (1% formic acid) and mobile phase B (1% formic acid/acetonitrile) delivered at 0.3 mL/min: 90% A/10% B (0 min)–70% A/30% B (8 min). The MS parameters were the same as for the analyses using the chiral column described above.

#### Animal experiments

The animal experimental model was designed as shown in our previous reports [33, 34]. All experiments were carried out with the approval of the Committee for Animal Care and Use of the National Institute of Health Sciences, Japan. Dextromethorphan hydrobromide (dissolved in an isotonic sodium chloride solution, 2.5 mg/mL, rat 1–3) or levome-

thorphan (dissolved in a mixed solution of 5% Emulphor™ EL-620/5% ethanol/90% isotonic sodium chloride solution, 2.5 mg/mL, rat 4–6) was administered to male DA pigmented rats, which were 5 weeks old and around 90 g mean weight (Japan SLC, Shizuoka, Japan). The drugs were given once daily at 5 mg/kg by intraperitoneal injection for ten successive days. Blood samples were collected 5, 15, 30, 60, 120, and 360 min after the first administration from the orbital vein plexus. Plasma samples were prepared by centrifugation at 10,000×g for 3 min and stored at –20 °C until analysis. The area under the plasma concentration time curve (AUC) was calculated by the conventional method. Urine samples were collected 0–24, 24–48, and 48–72 h after the last administration and stored at –20 °C. Each animal had been shaved on the back just before the first drug administration. The new growing hair samples were collected 28 days after the first administration.

#### Extraction of parent compounds and their metabolites from rat plasma and urine samples

For the quantitative analysis of *O*-demethyl and *N*, *O*-didemethyl metabolites in the rat plasma and urine samples, the analytes were measured as free compounds after the hydrolysis of *O*-glucuronides. The optimal condition of the hydrolysis was evaluated, with the peak of putative *O*-glucuronide at nearly 2 min (*m/z* 434→258) on the MRM chromatogram disappearing from rat plasma and urine samples after the hydrolysis.

A 25-μL plasma sample with 50 μL of added 10 mM ammonium formate buffer (pH 5.0) was reacted with 20 μL of the β-glucuronidase solution at 37 °C for 20 h. To precipitate the proteins in the plasma, 40 μL of the IS methanol solution and 100 μL of methanol were poured into each tube, and the mixtures were then vigorously mixed. The

**Table 1** Analytical conditions of LC-MS/MS using the Chiral CD-Ph column

Compounds	Retention time min	Precursor ions <i>m/z</i>	Cone voltage V	Product ions <i>m/z</i>	Collision energy eV
Dextromethorphan	10.6	272	40	171	45
Dextrorphan	6.1	258	45	157	40
(+)-3-MEM	8.1	258	40	170	35
(+)-3-HM	3.9	244	30	156	35
Levomethorphan	11.3	272	40	171	45
Levorphanol	5.5	258	45	157	40
(-)-3-MEM	9.8	258	40	170	35
(-)-3-HM	4.5	244	30	156	35
Levallorphan (IS)	7.5	284	40	157	40

mixed solution was centrifuged at 1,200×g for 3 min and filtered prior to the injection for the LC-MS/MS analysis.

To a 50- $\mu$ L urine sample (20  $\mu$ L for 0–24 h samples) was added 100  $\mu$ L of the  $\beta$ -glucuronidase solution, 1 mL of 10 mM ammonium formate buffer (pH 5.0) and 50  $\mu$ L of the IS aqueous solution, respectively. The mixed solution was incubated at 37 °C with gentle shaking. After an OASIS HLB column was pre-activated with 2 mL of methanol and distilled water, the reaction mixture was applied to the column. Following the wash of the column with 2 mL of distilled water, 1 mL of methanol was passed through the column to elute the target drugs. A 2- $\mu$ L of the solution was automatically injected into the UPLC-MS/MS.

#### Extraction of parent compounds and their metabolites from rat hair samples

Hair samples were washed three times with 0.1% sodium dodecyl sulfate under ultrasonication, followed by washing three times with water under the same condition. After the sample was dried under a nitrogen stream at room temperature, approximately 10 mg of finely cut hair was precisely weighed and extracted with 1 mL of methanol/5 M hydrochloric acid mixed solution (20:1) containing 50  $\mu$ L of the IS methanol solution for 1 h under ultrasonication. Following overnight storage at room temperature, the hair was filtered off, the filtrate was evaporated with a nitrogen stream, and the residue was dissolved in 1 mL of distilled water. The solution was treated with an OASIS HLB column and analyzed as described above.

#### Linearity, precision, and recovery of the analytical method for the rat samples

An individual standard solution of 1.0 mg/mL of each drug, dextromethorphan, levomethorphan, dextrorphan, 3-

hydroxymorphinan, 3-methoxymorphinan, and levorphanol, was prepared in methanol and stored at 4 °C. The IS solutions of 1  $\mu$ g/mL of levallorphan in methanol for the analysis of hair samples and those of 1  $\mu$ g/mL of levallorphan in distilled water for plasma and urine samples were also prepared.

The drug concentrations in the samples were calculated using the peak–area ratios of the ions monitored for the target compounds versus IS. The calibration curves for the determination were constructed by analyzing extracted drug-free control samples spiked with the standard solution, as described above. The calibration samples containing 0, 1, 2, 4, 20, 40, 200, and 400 ng/mL of the target drugs for the rat plasma, 0, 5, 10, 50, 100, 500, 1,000, 2,500, 5,000, and 10,000 ng/mL for the urine samples and 0, 0.1, 0.5, 1.0, 5.0, 10, 25, and 50 ng/mg for the hair samples were prepared just before analysis. The limit of quantitation (LOQ) of each drug was chosen to be the concentration of the lowest calibration standard with an acceptable limit of variance, while the limit of detection (LOD) was defined as concentrations in a sample matrix resulting in peak areas with signal-to-noise ratios (*S/N*) of 3.

The precision of the method was evaluated by five consecutive analyses of the plasma and urine samples that were spiked with the standard solutions containing 2, 20, and 200 ng/mL for the rat plasma samples and 5, 500, and 5,000 ng/mL for the urine samples, respectively. For the hair analyses, the control samples spiked with the standard solutions each containing 0.1, 5, and 50 ng/mg of the targeted drugs were evaluated. The recoveries of the four analytes from the rat samples were determined using each sample spiked with the analytes at a concentration of 80 ng/mL for the plasma, 500 ng/mL for the urine, and 10 ng/mg for the hair, respectively. To determine the recoveries, the responses of the analytes in the standard solutions and in the extracts from the rat control samples were compared. For the quantitative analysis of (–)-MEM and (–)-HM, the calibration curves of (+)-MEM and (+)-HM were used.

## Demethylation of dextromethorphan/levomethorphan in rat and human liver microsomes

For the *in vitro* experiments with rat and human liver microsomes, the reaction mixture consisted of 0.1 M potassium phosphate buffer (pH 7.4) with an NADPH generating system (1.3 mM NADP, 3.3 mM G-6-P, 0.4 U/mL G-6-PDH, 3.3 mM MgCl<sub>2</sub>), 50 μM substrate (dextromethorphan or levomethorphan), and 0.5 mg protein/mL microsomes (rat or human liver microsomes) in a final volume of 200 μL. Dextromethorphan and levomethorphan were dissolved in methanol, and the final concentration of the organic solvent was 0.1%. The incubation was started by adding the microsomal fraction and then continued for 0, 5, 10, or 20 min. The reaction was terminated by adding an equal volume of a mixed organic solution of 50% acetonitrile and 50% methanol, including 10 μM levallorphan (IS), and vigorous shaking. At the same time, a reaction mixture without the microsomal fraction was also incubated as an enzyme-free control. The mixture was centrifuged at 3,500×g for 3 min at 4 °C, and the supernatant was filtered prior to the injection for the LC-MS/MS analysis. The *in vitro* experiments for kinetic analyses were also performed as described above, except that 2, 5, 10, 50, 100, and 150 μM of substrates were incubated with the rat and human liver microsomes for 10 min. Each experiment was performed in duplicate and kinetic parameters were calculated with Eadie–Hofstee plots.

The results of the *in vitro* experiments were each evaluated by three consecutive analyses. The amounts of dextromethorphan/levomethorphan and their metabolites were calculated on the basis of calibration curves made by spiking known amounts of these compounds

into the reaction mixture without the microsomal fraction.

## Results

## Chiral separation of dextromethorphan/levomethorphan and their metabolites

Complete chiral separation of dextromethorphan, levomethorphan, and their metabolites was achieved in 12 min on a Chiral CD-Ph column in 0.1% formic acid–acetonitrile by a linear gradient program. The retention time of each compound was as follows: the parent compounds (dextro/levo forms, 10.6/11.3 min) and their metabolites of *O*-demethyl (6.1/5.5 min), *N*-demethyl (8.1/9.8 min), and *O*, *N*-didemethyl (3.9/4.5 min) as shown in Table 1. Figure 3 shows LC-MS/MS total ion current chromatograms (MRM mode) of the extract from plasma (30 min after the first administration), urine (0–24 h after the last administration), and hair (collected 4 weeks after the first administration) of rats administered with dextromethorphan or levomethorphan. Under the chromatographic conditions used, there was no interference with any of the compounds or the internal standard by any extractable endogenous materials in the rat samples. The peaks 7 (9.8 min, *m/z* 258→170) and 8 (4.5 min, *m/z* 244→156) on the chromatograms shown in Fig. 3 were identified as those of (–)-3-MEM and (–)-3-HM when the mass fragmentations of these peaks were considered, although the standard compounds of these two metabolites were not available. These peaks were also confirmed by comparison of their retention times and mass fragmentations with those of the standard compounds of the dextro forms ((+)-3-MEM and (+)-3-HM) using an ODS column.

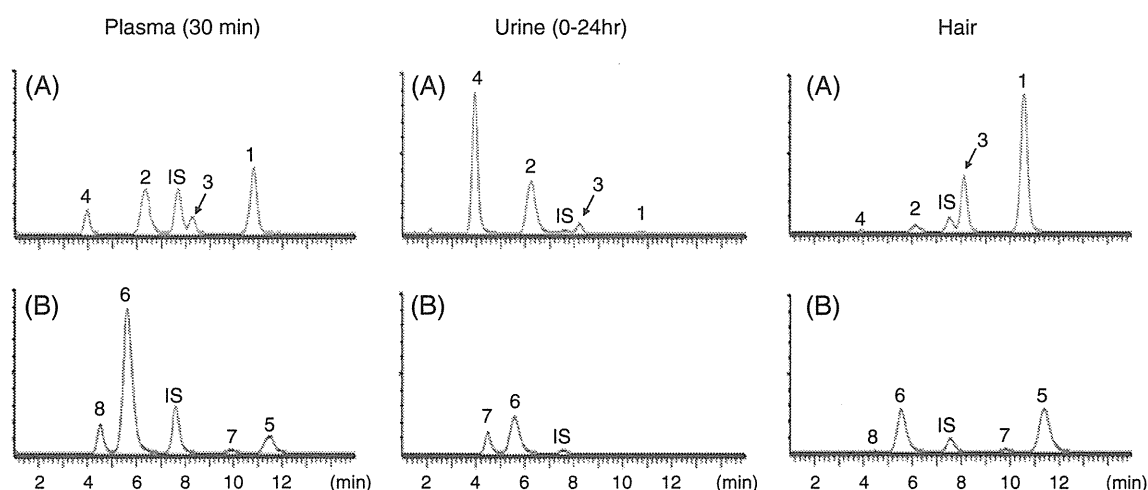


**Fig. 3** LC-MS/MS total ion current (TIC) chromatograms (MRM mode) of the extracts from plasma, urine, and hair of rats administered with (A) dextromethorphan and (B) levomethorphan using a chiral

column. 1 Dextromethorphan, 2 Dextrorphan, 3 (+)-3-MEM, 4 (+)-3-HM, 5 Levomethorphan, 6 Levorphanol, 7 (–)-3-MEM, 8 (–)-3-HM

**Table 2** Validation of results of the LC-MS/MS analyses of dextromethorphan/levomethorphan and their metabolites in rat plasma, urine and hair samples ( $n=5$ )

Samples	Compounds	LOD (S/N>3)	LOQ (S/N>10)	Linear ranges	Recoveries (%)	Precision (%) ( $n=5$ )			Accuracy (%) ( $n=5$ )				
						2.0 ng/mL	20 ng/mL	200 ng/mL	2.0 ng/mL	20 ng/mL	200 ng/mL		
Plasma (50 $\mu$ L)	Dextro	Dextromethorphan	0.8	1.0		80 ng/mL	22.1	9.3	1.5	-19.2	5.5	-0.2	
		Dextrorphan	0.4	0.8	1.0-400	81.7	10.2	3.8	1.5	10.2	2.2	-3.6	
		(+)-3-MEM	0.8	1.0		110.5	15.0	3.2	2.5	23.5	2.1	2.6	
		(+)-3-HM	0.8	1.0		92.5	15.7	6.1	1.8	13.7	-8.3	2.9	
	Levo	Levomethorphan	0.8	1.0	1.0-400	100.8	8.6	4.9	2.5	21.6	-4.4	-5.7	
		Levorphanol	0.8	1.0		90.7	15.9	4.1	2.3	-10.6	-5.6	-3.6	
		Dextromethorphan				(ng/mL)	500 ng/mL	5.0 ng/mL	500 ng/mL	5000 ng/mL	5.0 ng/mL	500 ng/mL	5000 ng/mL
		Dextromethorphan	1.0	2.5		90.2	9.7	0.8	2.6	-4.8	-5.2	-4.8	
Urine (100 $\mu$ L)	Dextro	Dextrorphan	1.0	2.5	5.0-10000	106.1	23.6	4.6	3.2	-17.9	11.1	-3.3	
		(+)-3-MEM	2.5	5.0		102.5	19.7	6.1	4.2	10.4	-5.8	2.7	
		(+)-3-HM	2.5	5.0		91.3	24.6	5.1	2.6	1.6	-9.9	1.5	
		Levomethorphan	1.0	5.0	10-10000	94.6	10.9	9.5	2.6	-4.3	-17.0	-2.2	
	Levo	Levorphanol	1.0	5.0		93.1	4.8	4.5	4.6	18.6	-8.0	6.8	
		Dextromethorphan				(ng/mg)	10 ng/mg	0.1 ng/mg	5.0 ng/mg	50 ng/mg	0.1 ng/mg	5.0 ng/mg	50 ng/mg
		Dextromethorphan	0.025	0.05		84.2	11.5	4.5	2.8	4.6	18.8	-6.6	
		Dextromethorphan	0.025	0.05	0.1-50	99.8	6.4	2.6	2.7	3.7	15.4	-3.5	
Hair (10 mg)	Dextro	(+)-3-MEM	0.025	0.05		83.8	18.6	3.9	1.5	4.7	0.6	-2.2	
		(+)-3-HM	0.025	0.1		91.4	11.2	6.2	2.8	4.6	18.8	-6.6	
		Levomethorphan	0.025	0.1	0.1-50	98.1	9.9	9.8	5.5	0.1	-2.3	-5.1	
		Levorphanol	0.025	0.05		112.2	8.8	2.8	4.2	11.9	1.3	-3.8	

Linearity and precision of the analytical method for the rat urine, plasma, and hair samples

The calibration curves were linear over the concentration range 1.0–400 ng/mL for rat plasma, 5.0–10,000 ng/mL (compounds of dextro forms) and 10.0–10,000 ng/mL (compounds of levo forms) for rat urine, and 0.1–50 ng/mg for rat hair, with good correlation coefficients of  $r^2 \geq 0.996$ , respectively. The LOD of each drug was 0.4 or 0.8 ng/mL for the plasma, 1.0 or 2.5 ng/mL for the urine, and 25  $\mu$ g/mg for the hair samples. The recoveries and the precision and accuracy data from the analytical procedures for the rat samples ( $n=5$ ), spiked with a standard solution of the targeted compounds, are shown in Table 2.

Determination of dextromethorphan/levomethorphan and their metabolites in DA rat plasma, urine, and hair samples

It has been reported that a female DA rat lacks the CYP2D1 enzyme, which is known to be related to *O*-demethylation of dextromethorphan in the SD rat; it is therefore used as a model animal for the poor metabolizer phenotype of dextromethorphan [35–37]. As such, the metabolic data from female DA rats may not reflect the “normal” situation. On the other hand, pigmented hairy rats appear to be suitable for the investigation of analytical methods of basic drugs in hair samples, compared with albino rats (SD or Wistar rats) because pigmentation (the melanin contents) is one of the most important factors regarding the incorpora-

tion of basic drugs into hair, as described before [38]. Therefore, thus far, we have studied the analytical properties of various drugs in hair samples using the pigmented hairy male DA rats, avoiding female DA rats.

After the i.p. administration of dextromethorphan or levomethorphan to pigmented hairy male DA rats, the parent compounds and their three metabolites in the plasma, urine, and hair were determined using LC-MS/MS. The optical purities of the resulting metabolites were unchanged in any rat biological sample, and no racemation was observed through *O*- and/or *N*-demethylation (Fig. 3). In the rat plasma ( $AUC_{50-360 \text{ min}}$ ) and urine samples (total excretions for 0–72 h) after the hydrolysis of *O*-glucuronides, most metabolites were detected as being the corresponding *O*-demethyl and *N*, *O*-didemethyl compounds, as shown in Table 3. However, obvious differences in the amounts of these metabolites were found between the dextro and levo forms. After administration of dextromethorphan, dextrorphan and (+)-3-HM were the major metabolites in the plasma (59.4 and 64.3 mg/L·min) and urine (106.1 and 226.9  $\mu$ g/mL). However, *O*-demethyl metabolites (levorphanol) were mainly detected in the plasma (197.1 mg/L·min) and urine (210.5  $\mu$ g/mL) after administration of levomethorphan (Table 3).

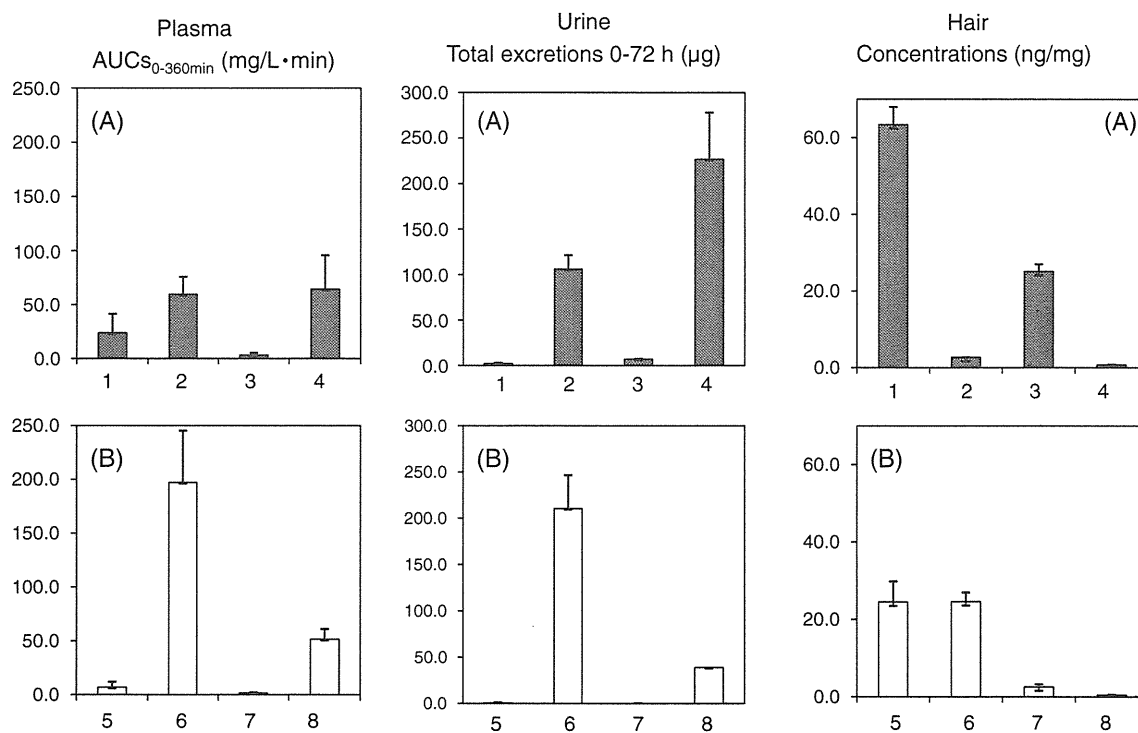
In the hair samples, the differences in the amounts of the metabolites are more clearly detected. After administration of dextromethorphan, the parent compound and the *N*-demethyl metabolite ((+)-3-MEM) were mainly detected at 63.4 and 25.1 ng/mg, respectively, although the *O*-demethyl metabolite of dextromethorphan (dextrorphan) was detected at only 2.70 ng/mg, which was nearly one tenth of the level

**Table 3** Rat plasma AUC<sub>0–360min</sub>, total excretion into rat urine, and concentrations in rat hair of dextromethorphan/levomethorphan and their metabolites

Administrations	Targeted compounds	Plasma AUC <sub>0–360min</sub> (mg/L·min)	Urine Total excretion 0–72 h (μg)	Hair Concentration (ng/mg)
Dextromethorphan (rat 1–3)	Dextromethorphan	23.8±17.6	2.13±1.05	63.4±4.6
	Dextrorphan	59.4±16.3	106.1±15.3	2.70±0.04
	(+)-3-MEM	3.10±2.15	6.95±0.68	25.1±1.9
	(+)-3-HM	64.3±31.3	226.9±51.3	0.70±0.11
Levomethorphan (rat 4–6)	Levomethorphan	6.90±5.12	0.59±0.61	24.5±5.3
	Levorphanol	197.1±48.2	210.5±36.2	24.6±2.4
	(-)-3-MEM	1.47±0.64	0.13±0.06	2.57±0.71
	(-)-3-HM	51.5±9.6	39.0±5.9	0.49±0.09

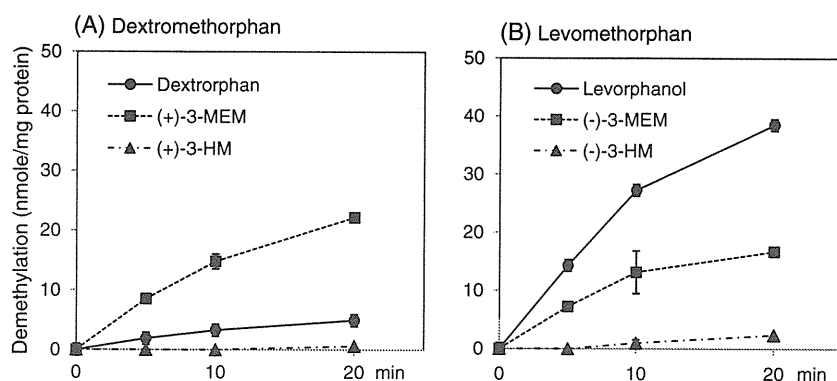
of levorphanol. In contrast, after the administration of levomethorphan, the parent compound and the *O*-demethyl metabolite (levorphanol) were mainly detected at 24.5 and 24.6 ng/mg, respectively, with a small amount of the *N*-demethyl metabolite ((-)-3-MEM). The *N*, *O*-didemethyl metabolites (3-HM) were hardly detected in either sample (Table 3). The ratios of the parent compounds, their *O*-demethyl, *N*-demethyl, and *N*, *O*-didemethyl metabolites in the hair samples were 100:4:40:1 for the dextro forms and 100:100:11:2 for the levo forms, respectively.

The rat plasma AUCs, total excretions into rat urine and concentrations in rat hair of dextromethorphan or levomethorphan, and their metabolites are summarized in Fig. 4. The metabolic ratios of dextromethorphan/levomethorphan, *O*-demethyl, *N*-demethyl, and *N*, *O*-didemethyl metabolites in rat plasma (AUC<sub>0–360 min</sub>) and hair (collected 4 weeks after the first administration) were 1:3:0.1:3 and 1:0.04:0.4:0.01 for the dextro forms and 1:29:0.2:7 and 1:1:0.1:0.02 for the levo forms, respectively. It is of interest that the concentrations of dextromethorphan and levome-

**Fig. 4** Rat plasma AUC<sub>0–360min</sub>, total excretions into rat urine, and concentrations in rat hair of parent compounds and their metabolites after administration of (A) dextromethorphan and (B) levomethor-

phan. 1 Dextromethorphan, 2 Dextrorphan, 3 (+)-3-MEM, 4 (+)-3-HM, 5 Levomethorphan, 6 Levorphanol, 7 (-)-3-MEM, 8 (-)-3-HM

**Fig. 5** Demethylation of (A) dextromethorphan and (B) levomethorphan in DA rat liver microsomes



thorphan in the rat hair were obviously high compared with those in the plasma, while those of their *O*-demethyl and *N*, *O*-didemethyl metabolites in the hair (which mostly existed as very hydrophilic metabolites, *O*-glucuronides in the plasma) were extremely low considering their high plasma AUCs.

#### Demethylation of dextromethorphan/levomethorphan in DA rat liver microsomes

In order to fully investigate the differences of the metabolic properties between dextromethorphan and levomethorphan, DA rat liver microsomes were studied. Figure 5 shows the *O*- and/or *N*-demethylation of dextromethorphan/levomethorphan in the rat liver microsomes.

The optical purities of the resulting metabolites were unchanged in the liver microsomes, and no racemation was observed through *O*- and/or *N*-demethylation. After 20-min incubation, 4.8% of dextromethorphan and 45% of levomethorphan were transformed to each *O*-demethyl metabolite, and 22% and 19% of the parent compounds were transformed to each *N*-demethyl metabolite. The *N*-demethylation was preferred over *O*-demethylation for dextromethorphan. In contrast, *O*-demethylation was preferred over *N*-demethylation for levomethorphan and the *O*-demethylation of levomethorphan was performed at levels 9.4 times that of dextromethorphan after 20-min incubation. The *N*-demethylation of levomethorphan was almost the same as that of dextromethorphan. Table 4 shows kinetic parameters for *O*-demethylation of dextromethorphan and levomethorphan by the DA rat microsomes. The  $V_{\max}$  value for levomethorphan ( $3.8 \pm$

$0.3 \text{ nmol/min/mg protein}$ ) was 5.9 times higher than that of dextromethorphan ( $0.65 \pm 0.03 \text{ nmol/min/mg protein}$ ). The  $K_m$  values for levomethorphan and dextromethorphan were  $22.1 \pm 5.0$  and  $44.1 \pm 4.0 \text{ } \mu\text{M}$ , respectively. These results suggest that there might be an enantioselective *O*-demethylation of levomethorphan in the DA rat liver microsomes. This enantioselective metabolism might be the cause of the different amounts of the metabolites observed in the rat plasma, urine, and hair after administration of dextromethorphan and levomethorphan.

#### Demethylation of dextromethorphan/levomethorphan in pooled human liver microsomes

In order to investigate whether the enantioselective metabolism could be observed in humans as well as in DA rats, the pooled human liver microsomes were examined. Figure 6 shows the *O*- and/or *N*-demethylation of dextromethorphan/levomethorphan in the human liver microsomes.

The optical purities of the resulting metabolites were unchanged also in the human liver microsomes, and no racemation was observed through *O*- and/or *N*-demethylation. After 20-min incubation, 3.3% of dextromethorphan and 11% of levomethorphan were transformed to each *O*-demethyl metabolite and 2.5% and 7.1% of the parent compounds were transformed to each *N*-demethyl metabolite. The total amounts of the three metabolites from levomethorphan were higher than those from dextromethorphan in human (3.1 times) microsomes. Kinetic parameters for *O*-demethylation of dextromethorphan and

**Table 4** Kinetic parameters for *O*-demethylation of dextromethorphan/levomethorphan by DA rat and human liver microsomes

	DA rat liver microsomes		Human liver microsomes	
	Dextromethorphan	Levomethorphan	Dextromethorphan	Levomethorphan
$V_{\max}$ (nmol/min/mg protein)	$0.65 \pm 0.03$	$3.8 \pm 0.3^a$	$0.26 \pm 0.03$	$0.58 \pm 0.02^a$
$K_m$ ( $\mu\text{M}$ )	$44.1 \pm 4.0$	$22.1 \pm 5.0^a$	$4.5 \pm 0.9$	$8.9 \pm 1.7^a$

<sup>a</sup>Significantly different from dextromethorphan ( $p < 0.01$ )

levomethorphan in the human liver microsomes are listed in Table 4. The  $V_{\max}$  value for levomethorphan ( $0.58 \pm 0.02$  nmol/min/mg protein) was 2.2 times higher than that of dextromethorphan ( $0.26 \pm 0.03$  nmol/min/mg protein). The  $K_m$  values for levomethorphan and dextromethorphan were  $8.9 \pm 1.7$  and  $4.5 \pm 0.8$   $\mu\text{M}$ , respectively. There could also be an enantioselective metabolism of levomethorphan in human liver microsomes.

## Discussion

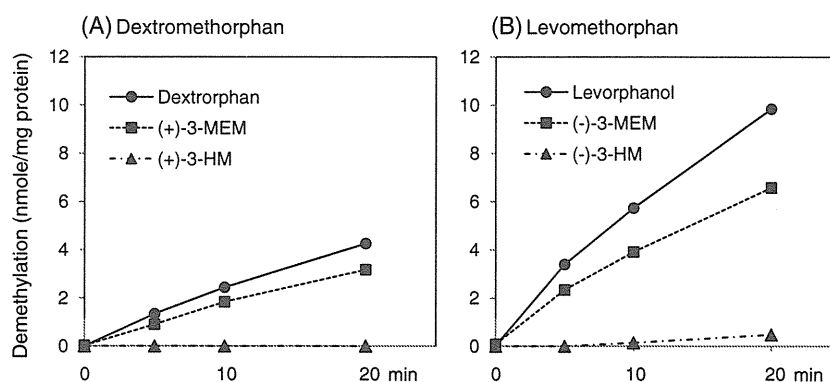
In this study, we first investigated the analytical methods of dextromethorphan/levomethorphan and their metabolites in biological samples using DA male rats. As a result, chiral separation of dextromethorphan, levomethorphan, and their metabolites in biological samples was achieved in 12 min on a Chiral CD-Ph column. The optical purities of the resulting metabolites were unchanged in all rat biological samples, and no racemation was observed through *O*- and/or *N*-demethylation. The proposed chiral analyses might be applied to human samples and could provide useful information for discriminating dextromethorphan use from levomethorphan use, considering the possibility of the adulteration or substitution of dextromethorphan with levomethorphan for illegal purposes. However, for application to forensic toxicological purposes, further studies should be carried out using authentic human samples.

The concentrations of dextromethorphan and levomethorphan in the rat hair were obviously high compared with those of metabolites in the plasma and urine samples in this study. In our previous study [38], we determined the melanin affinity and lipophilicity of 20 abused drugs and these values were compared with the ratio of drug concentration in hair to plasma AUC as an index of the incorporation tendency into hair. As a result, the combination of melanin affinity (basicity) and lipophilicity showed a high correlation with the incorporation tendency into hair. Parent compounds can be detected relatively easily in hair

in comparison with their hydrophilic metabolites. Actually, it has been reported that cocaine is detected in hair at a much higher concentration than its metabolite, benzoylecgonine, although cocaine is rapidly hydrolyzed to benzoylecgonine and disappears from plasma [39]. Considering those reports, the physico-chemical properties of dextromethorphan/levomethorphan and their metabolites could be significantly related to their concentrations in the hair samples. Additionally, the drug concentrations in the rat hair (collected 4 weeks after the first administration) reflected the total amounts of drugs in the plasma of rats administered with dextromethorphan/levomethorphan for ten successive days, and the differences might become more distinct. The detection of the parent compounds from hair samples would provide useful information regarding the monitoring of their use over a long period.

In the DA rat samples, obvious differences in the ratios of the metabolites were found between the dextro and levo forms. These differences were most clearly detected in the hair samples. The concentrations of the parent compounds, their *O*-demethyl, *N*-demethyl, and *N*, *O*-didemethyl metabolites were 63.4, 2.7, 25.1, and 0.7 ng/mg for the dextro forms and 24.5, 24.6, 2.6, and 0.5 ng/mg for the levo forms, respectively. In order to investigate the differences of their metabolic properties between dextromethorphan and levomethorphan, DA rat and human liver microsomes were studied. As a result, we have shown the enantioselective metabolism of levomethorphan, not only in DA rats but also in human liver microsomes, especially with regards to the *O*-demethylation. Because it is well-known that CYP2D6 (mainly related to *O*-demethylation of dextromethorphan) is polymorphically expressed in humans, it may be difficult to discuss the enantioselective metabolism in humans who can be classified as poor, intermediate and extensive metabolizers of dextromethorphan. In future studies, the metabolic properties of these drugs using CYP2D6 enzymes (having a variety of phenotypes) should be examined to clarify the effects of their genotypes on the enantioselective *O*-demethylation of levomethorphan observed in this study.

**Fig. 6** Demethylation of (A) dextromethorphan and (B) levomethorphan in human liver microsomes



## Conclusions

In this present study, we have established procedures for chiral analyses of dextromethorphan, levomethorphan, and their *O*-demethyl and/or *N*-demethyl metabolites in rat plasma, urine, and hair using LC-MS/MS. These analytical methods might be applied to human samples and could be useful for discriminating dextromethorphan use from levomethorphan use although further studies should be carried out using authentic human samples for forensic toxicological purposes. In addition, we have found the enantioselective metabolism of levomethorphan, not only in DA rats but also in human liver microsomes, especially with regards to the *O*-demethylation. This is the first report describing the differences in metabolic properties between dextromethorphan and levomethorphan in rats and humans.

**Acknowledgments** Part of this work was supported by a Health and Labor Sciences Research Grant from the Ministry of Health, Labor and Welfare in Japan.

## References

- Mutschler J, Koopmann A, Grosshans M, Hermann D, Mann K, Kiefer F (2010) *Dtsch Arztebl Int* 107:537–540
- Chyka PA, Erdman AR, Manoguerra AS, Christianson G, Booze LL, Nelson LS, Woolf AD, Cobaugh DJ, Caravati EM, Scharman EJ, Troutman WG (2007) *Clin Toxicol* 45:662–677
- Banken JA, Foster H (2008) *Ann NY Acad Sci* 1139:402–411
- Shin EJ, Lee PH, Kim HJ, Nabeshima T, Kim HC (2008) *J Pharmacol Sci* 106:22–27
- Bryner JK, Wang UK, Hui JW, Bedodo M, MacDougall C, Anderson IB (2006) *Arch Pediatr Adolesc Med* 160:1217–1222
- Miller SC (2005) *Addict Biol* 10:325–327
- Logan BK, Goldfogel G, Hamilton R, Kuhlman J (2009) *J Anal Toxicol* 33:99–103
- Rammer L, Holmgren P, Sandler H (1988) *Forensic Sci Int* 37:233–236
- Woods JW, Carney J (1978) *NIDA Res Monogr* 18:54–66
- Trescot AM, Datta S, Lee M, Hansen H (2008) *Pain Physician* 11: S133–S153
- Jacqz-Aigrain E, Funck-Brentano C, Cresteil T (1993) *Pharmacogenetics* 3:197–204
- Schmid B, Bircher J, Preisig R, K pfer A (1985) *Clin Pharmacol Ther* 38:618–624
- Gorski JC, Jones DR, Wrighton SA, Hall SD (1994) *Biochem Pharmacol* 48:173–182
- K ppel C, Tenczer J, Arndt I, Ibe K (1987) *Arzneimittelforschung* 37:1304–1306
- Lutz U, Bittner N, Lutz RW, Lutz WK (2008) *J Chromatogr B* 871:349–356
- Kristensen HT (1998) *J Pharm Biomed Anal* 18:827–838
- Aumatell A, Wells RJ (1993) *J Chromatogr Sci* 31:502–508
- Lin SY, Chen CH, Ho HO, Chen HH, Sheu MT (2007) *J Chromatogr B* 859:141–146
- Bendriess EK, Markoglou N, Wainer IW (2001) *J Chromatogr B* 754:209–215
- Afshar M, Rouini MR, Amini M (2004) *J Chromatogr B* 802:317–322
- Hendrickson HP, Gurley BJ, Wessinger WD (2003) *J Chromatogr B* 788:261–268
- Kim SC, Chung H, Lee SK, Park YH, Yoo YC, Yun YP (2006) *Forensic Sci Int* 161:185–188
- Spanakis M, Vizirianakis IS, Mironidou-Tzouveleki M, Niopas I (2009) *Biomed Chromatogr* 23:1131–1137
- Rodrigues WC, Wang G, Moore C, Agrawal A, Vincent MJ, Soares JR (2008) *J Anal Toxicol* 32:220–226
- Kim EM, Lee JS, Park MJ, Choi SK, Lim MA, Chung HS (2006) *Forensic Sci Int* 161:198–201
- Bagheri H, Es-haghi A, Rouini MR (2005) *J Chromatogr B* 818:147–157
- Eichhold TH, McCauley-Myers DL, Khambe DA, Thompson GA, Hoke SH 2nd (2007) *J Pharm Biomed Anal* 43:586–600
- Kuhlenbeck DL, Eichold TH, Hoke SH 2nd, Baker TR, Mensen R, Wehmeyer KR (2005) *Eur J Mass Spectrom* 11:199–208
- Lutz U, V lkel W, Lutz RW, Lutz WK (2004) *J Chromatogr B* 813:217–225
- Vengurlekar SS, Heitkamp J, McCush F, Velagaleti PR, Brisson JH, Bramer SL (2002) *J Pharm Biomed Anal* 30:113–124
- Sunouchi M, Fukuhara M, Ohno Y, Takanaka A (1988) *J Toxicol Sci* 13:193–204
- Ozawa S, Ohta K, Miyajima A, Kurebayashi H, Sunouchi M, Shimizu M, Murayama N, Matsumoto Y, Fukuoka M, Ohno Y (2000) *Xenobiotica* 10:1005–1017
- Kikura-Hanajiri R, Kawamura M, Saisho K, Kodama Y, Goda Y (2007) *J Chromatogr B* 855:121–126
- Kikura-Hanajiri R, Kawamura M, Miyajima A, Sunouchi M, Goda Y (2010) *Forensic Sci Int* 198:62–69
- Bochner F, Somogyi AA, Chen ZR (1994) *Xenobiotica* 24:543–552
- Kerry NL, Somogyi AA, Mikus G, Bochner F (1993) *Biochem Pharmacol* 45:833–839
- Zysset T, Zeugin T, K pfer A (1988) *Biochem Pharmacol* 37:3155–3160
- Nakahara Y, Takahashi K, Kikura R (1995) *Biol Pharm Bull* 18:1223–1227
- Nakahara Y, Ochiai T, Kikura R (1992) *Arch Toxicol* 66:446–449



# Molecular Responses of Human Lung Epithelial Cells to the Toxicity of Copper Oxide Nanoparticles Inferred from Whole Genome Expression Analysis

Nobutaka Hanagata,<sup>†,‡,\*</sup> Fei Zhuang,<sup>‡,§</sup> Sarah Connolly,<sup>†,||</sup> Jie Li,<sup>†</sup> Nobuhiro Ogawa,<sup>§</sup> and Mingsheng Xu<sup>†</sup>

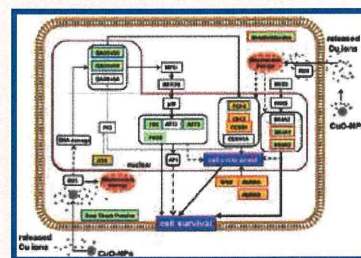
<sup>†</sup>Nanotechnology Innovation Station, National Institute for Materials Science, 1-2-1 Sengen, Tsukuba, Ibaraki 305-0047, Japan, <sup>‡</sup>Graduate School of Life Science, Hokkaido University, N10W8, Kita-ku, Sapporo 060-0812, Japan, <sup>§</sup>Biomaterials Unit, National Institute for Materials Science, 1-2-1 Sengen, Tsukuba, Ibaraki 305-0047, Japan, and <sup>||</sup>State Key Laboratory of Silicon Materials, MOE Key Laboratory of Macromolecule Synthesis and Functionalization, and Department of Polymer Science and Engineering, Zhejiang University, Hangzhou 310027, People's Republic of China. <sup>||</sup>Present address: Microbiology and Cell Science, University of Florida, Gainesville, Florida 32611-0700.

As a result of recent advances in nanotechnology, the industrial use of nanomaterials is increasing. Although the size, shape, surface area, and surface activity of nanomaterials are attractive for many different applications, concern exists that these properties may contribute to the toxicity of nanomaterials. For example, their small size could allow them to easily enter the body through respiratory passages or wounds and affect various tissues. However, clear safety standards have not been established for nanomaterials.

Previously, we demonstrated that copper oxide nanoparticles (CuO-NPs) are the most toxic metal oxide nanoparticles.<sup>1,2</sup> CuO-NPs are used in textiles for their antibacterial effects.<sup>3</sup> They are also being developed for use in catalysts, gas sensors, microelectronic materials, and cosmetics.<sup>4,5</sup> Furthermore, Cu-NPs are added as materials to ink, plastics, lubricants, metallurgical coatings, and cosmetics for the skin.<sup>6</sup> Although SiO<sub>2</sub>-NPs (15–25 nm), CeO<sub>2</sub>-NPs (20 nm), and Al<sub>2</sub>O<sub>3</sub>-NPs (15–50 nm) are not toxic to A549 cells, ZnO-NPs (20–60 nm) are cytotoxic to a lesser extent than CuO-NPs.<sup>1,2</sup>

These findings suggest that the toxicity of metal oxide nanoparticles is not due to their size but their chemical composition. Specifically, metal oxide nanoparticles such as CuO-NPs and ZnO-NPs that release metal ions are most likely to be cytotoxic. In addition to CuO-NPs and ZnO-NPs, Ag-NPs are highly cytotoxic to HeLa cervical cancer cells, and Ag ions that are released into the culture medium are responsible for much of the toxicity.<sup>7</sup> However, until recently, the

**ABSTRACT** This study proposes a molecular mechanism for lung epithelial A549 cell response to copper oxide nanoparticles (CuO-NPs) related to Cu ions released from CuO-NPs. Cells that survived exposure to CuO-NPs arrested the cell cycle as a result of the downregulation of proliferating cell nuclear antigen (PCNA), cell division control 2 (CDC2), cyclin B1 (CCNB1), target protein for Xklp2 (TPX2), and aurora kinase A (AURKA) and B (AURKB). Furthermore, cell death was avoided through the induced expression of nuclear receptors NR4A1 and NR4A3 and growth arrest and DNA damage-inducible 45  $\beta$  and  $\gamma$  (GADD45B and GADD45G, respectively). The downregulation of CDC2, CCNB1, TPX2, AURKA, and AURKB, the expressions of which are involved in cell cycle arrest, was attributed to Cu ions released from CuO-NPs into medium. NR4A1 and NR4A3 expression was also induced by Cu ions released into the medium. The expression of GADD45B and GADD45G activated the p38 pathway that was involved in escape from cell death. The upregulation of GADD45B and GADD45G was not observed with Cu ions released into medium but was observed in cells exposed to CuO-NPs. However, because the expression of the genes was also induced by Cu ion concentrations higher than that released from CuO-NPs into the medium, the expression appeared to be triggered by Cu ions released from CuO-NPs taken up into cells. We infer that, for cells exposed to CuO-NPs, those able to make such a molecular response survived and those unable to do so eventually died.



**KEYWORDS:** copper oxide nanoparticles · cytotoxicity · lung epithelial cells · cell cycle arrest · DNA microarray

nanoparticles themselves, rather than released Cu ions, have been suggested to cause CuO-NP cytotoxicity.<sup>8,9</sup> The uptake of CuO-NPs into cells and subsequent generation of intracellular reactive oxygen species (ROS) have been reported to cause cytotoxicity and genotoxicity,<sup>8,10</sup> but the molecular basis of CuO-NP toxicity has not been clarified.

\* Address correspondence to hanagata.nobutaka@nims.go.jp.

Received for review May 10, 2011 and accepted November 11, 2011.

Published online November 11, 2011 10.1021/nn202966t

© 2011 American Chemical Society



Human lung epithelial A549 cells were used in this study because we have a greater chance of inhaling nanoparticles in the workplace rather than taking them up through the skin, ingestion, and injection. A549 cells that were derived from carcinoma tissue are classified as type I pneumocytes, which cover >95% of the internal surface that provides a barrier function and gas exchange in the lung. We used DNA microarrays to analyze the effects of CuO-NPs on the global gene expression of A549 cells. First, we identified genes affected by exposure to CuO-NPs and inferred functional changes of cells using gene ontology (GO) analysis, in which affected genes were classified into functional categories. Next, we performed global gene expression analysis of cells exposed to Cu ions released from CuO-NPs into medium and identified genes that were regulated by both CuO-NPs and released Cu ions. These analyses revealed the contribution of released Cu ions to the toxicity of CuO-NPs at the molecular level. Furthermore, we examined the gene expression of cells exposed to different concentrations of CuCl<sub>2</sub> to confirm the contribution of Cu ions released from CuO-NPs. Our results suggest that the *in vitro* cytotoxicity of CuO-NPs is primarily due to the effects of Cu ions that are released into the culture medium and absorbed into cells.

## RESULTS AND DISCUSSION

**Preparation and Characterization of Medium Containing Cu Ions Released from CuO-NPs.** The average diameter of CuO-NPs used in this study was 50 nm,<sup>1</sup> and the mean aggregate size of the particles after dispersal in medium at a concentration of 25 μg/mL was around 300 nm (Supporting Information Figure S1). However, CuO-NPs were immediately sedimented. The morphology and electronic properties of CuO-NPs have been reported previously.<sup>1</sup>

To investigate the contribution of the released Cu ions to the toxicity of CuO-NPs, we prepared culture medium containing Cu ions released from CuO-NPs (Supporting Information Figure S2a). CuO-NPs (25 μg/mL final concentration) were added to the culture medium and incubated at 37 °C for 24 h. Then, the medium containing CuO-NPs was centrifuged at 150 000g for 1 h to remove the CuO-NPs. Inductively coupled plasma optical emission spectrometry (ICP-OES) indicated that the Cu concentration in the resulting supernatant was 13.2 ± 1.54 μg/mL (11.6–15.0 μg/mL, *n* = 5). To examine the presence or absence of CuO-NPs in the supernatant, we analyzed the supernatant using a laser diffraction particle analyzer (DLS). The analysis revealed the presence of NPs in the supernatant (Figure 1a). However, the similar pattern of size distribution was also observed in the culture medium without CuO-NPs after incubation at 37 °C for 24 h (Figure 1b and Supporting Information Figure S2b), suggesting that the NPs in the supernatant are attributed to medium components, not CuO-NPs. In addition, as shown by transmission electron microscopy

(TEM) and energy-dispersive spectroscopy (EDS) (Figure 1c–f), NPs in the supernatant contained hardly any CuO-NPs. On the other hand, observation of the resulting precipitation that contains CuO-NPs removed from the culture medium, using scanning electron microscope (SEM), revealed CuO-NPs with smaller than original size (Figure 1g,h). This implies that CuO-NPs released Cu ions into the culture medium, resulting in smaller size. Therefore, we used the supernatant as the culture medium containing released Cu ions to assess the contribution of the released Cu ions to the toxicity of CuO-NPs. Although CuO-NPs released Cu ions into the medium, they hardly released the ions in water (Supporting Information Figure S2c).

**Toxicity of CuO-NPs.** The number of viable A549 cells cultured in 25 μg/mL CuO-NPs or the supernatant was 34 and 81% of that of the control culture, respectively (Figure 2a and Supporting Information Figure S3). This result indicated that released Cu ions are also toxic and may account for part of the toxicity of CuO-NPs. In addition, we used the water-soluble tetrazolium salt (WST) cell proliferation assay, which is based on the production of formazan from WST-8 by mitochondrial dehydrogenases in viable cells, to measure cytotoxicity. The amount of formazan produced by cells cultured in 25 μg/mL CuO-NPs or the supernatant was 20 and 57% of that of the control culture, respectively (Figure 2b). This result implies that the CuO-NPs and released Cu ions damaged the mitochondria. This damage occurred after 4 h of exposure to CuO-NPs (Supporting Information Figure S4). Furthermore, supplementation of Al<sub>2</sub>O<sub>3</sub>-NPs with 50 nm in size that were used as nontoxic dummy NPs to the supernatant did not affect the formazan formation of the supernatant (Supporting Information Figure S5), suggesting released Cu ions alone damaged mitochondria. Approximately 9% of cells underwent apoptosis in response to CuO-NPs, but we observed few apoptotic cells in culture with the supernatant (Figure 2c). These results suggested that CuO-NPs damaged mitochondria and induced apoptosis, and that released Cu ions were responsible for some of the damage to the mitochondria.

To confirm the contribution of released Cu ions to the toxicity of CuO-NPs, we examined the cytotoxicity of different concentrations of CuCl<sub>2</sub>. In cultures with the supernatant, the number of viable cells and the amount of formazan was 81 and 57% of control culture levels (Figure 2a,b). The concentration of CuCl<sub>2</sub> required for similar toxicity was 25–33 μg/mL (Figure 2d,e). This concentration is equivalent to 11.8–15.6 μg/mL Cu ions, which was consistent with the concentration of Cu ions that were released from CuO-NPs. This result showed that the effect of Cu ions that are released from CuO-NPs is similar to that of Cu ions from CuCl<sub>2</sub>.

Next, we examined the uptake of CuO-NPs into cells using TEM. NP-like structures were observed inside cell (Supporting Information Figure S6). To verify whether

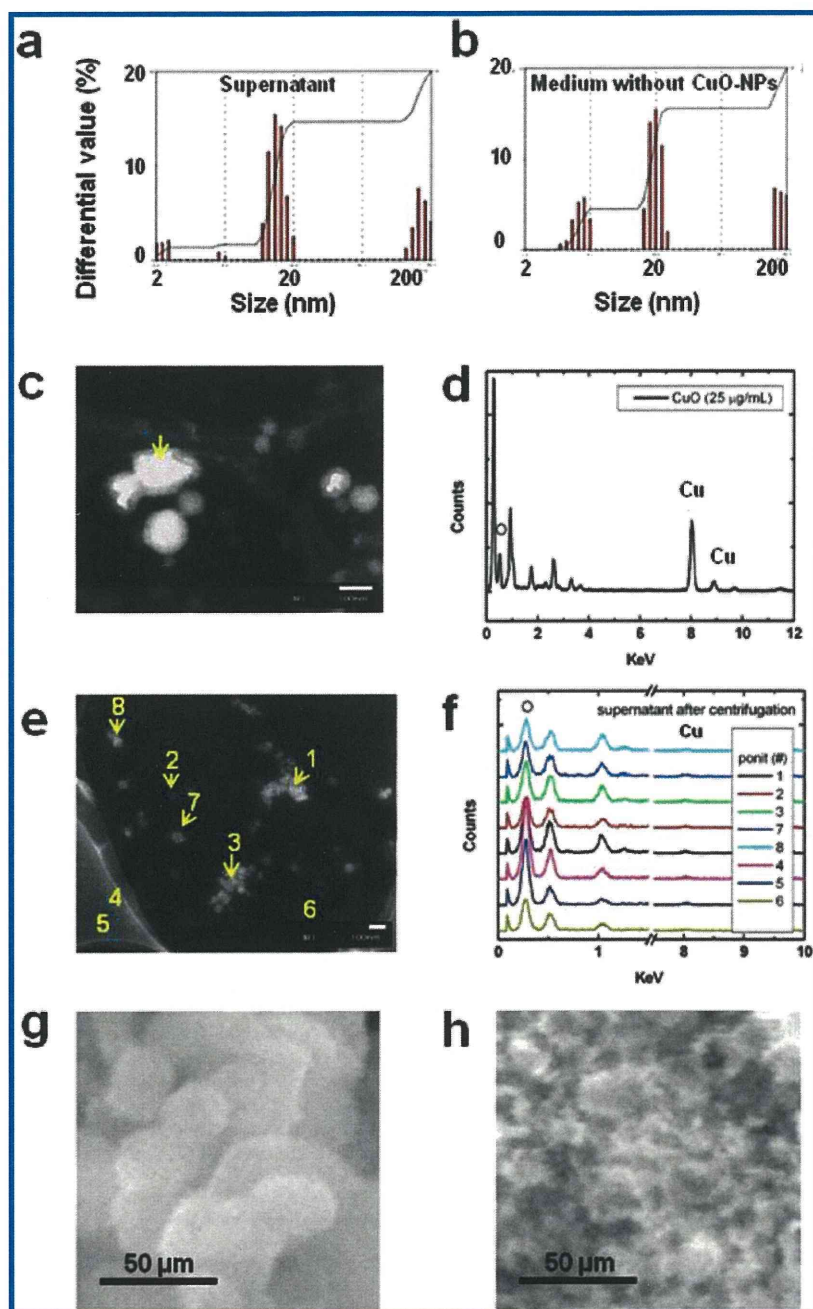


**Figure 1.** Characterization of supernatant for preparation of medium containing Cu ions released from CuO-NPs. (a) Size distribution of NPs in supernatant. (b) Size distribution of NPs in medium without CuO-NPs incubated at 37 °C for 24 h. (c) Dark-field TEM image of a CuO-NP sample. A TEM grid was immersed into the cell culture medium that contained 25 μg/mL CuO-NPs and then air-dried. (d) EDS spectrum of the point indicated by the arrow in (c), which suggests the presence of Cu and O. (e) Dark-field TEM image of the supernatant. The CuO-NP suspension was centrifuged at 150 000g for 1 h. Subsequently, a TEM grid was immersed into the supernatant and then air-dried. (f) EDS spectra of points 1–8 in (e). (g) SEM image of original CuO-NPs. (h) SEM image of CuO-NPs incubated in medium at 37 °C for 24 h.

these NP-like structures are attributed to CuO-NPs, elemental maps were analyzed. The elemental maps clearly showed that CuO-NPs were taken up into cell (Figure 3).

**Molecular Response of Cells to CuO-NPs.** To elucidate the underlying molecular mechanism of CuO-NP toxicity, comprehensive gene expression analysis was performed using DNA microarray. We exposed A549 cells to 25 μg/mL CuO-NPs for 24 h and then identified

genes that demonstrated greater than 2-fold change in expression level compared with those in control cells. Our results revealed that CuO-NPs upregulated the expression of 648 genes and downregulated the expression of 562 genes. These data have been deposited in the Gene Expression Omnibus database with accession code G33278. By classifying these genes into GO functional categories, we obtained the following statistically significant categories ( $p < 0.001$ ): CuO-NPs upregulated genes



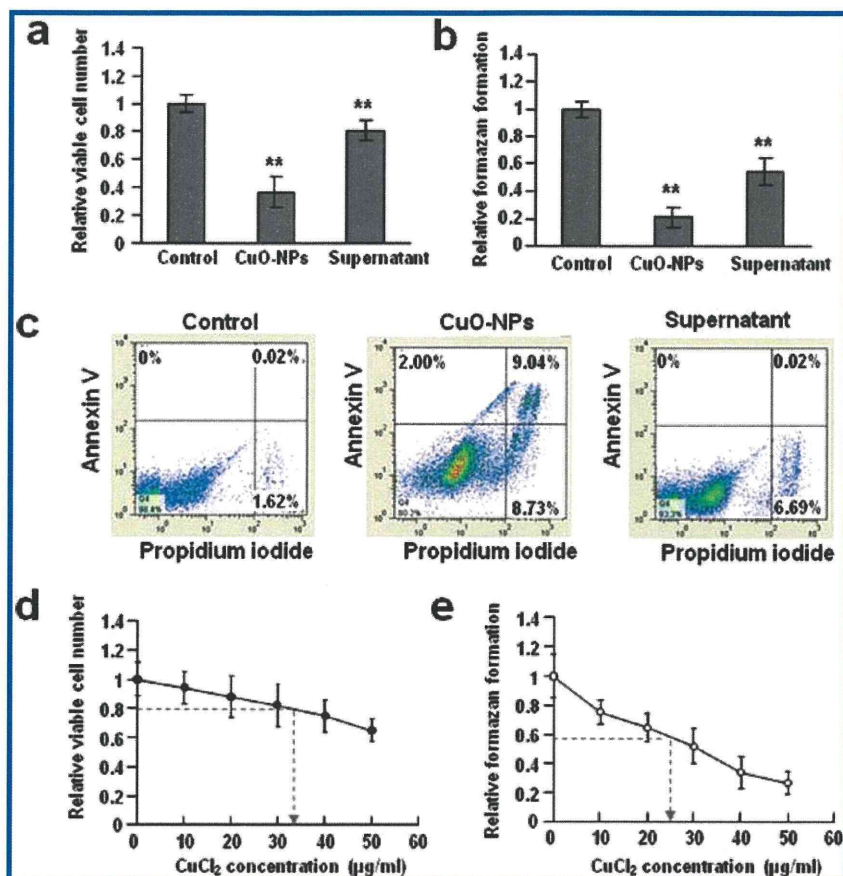


**Figure 2.** Toxicity of CuO-NPs and released Cu ions. (a) Cytotoxicity of CuO-NPs and supernatant as indicated by the number of viable cells. A549 human lung epithelial cells were cultured in media containing 25  $\mu\text{g}/\text{mL}$  CuO-NPs or supernatant at 37  $^{\circ}\text{C}$  for 24 h, and then the number of viable cells was compared to that of control (untreated) cells (defined as 1). Results are expressed as mean (SE) ( $n = 4$ );  $**p < 0.05$ . (b) Cytotoxicity of CuO-NPs and supernatant as indicated by cell viability in the WST assay. Results are expressed as mean (SE) ( $n = 8$ );  $**p < 0.05$ . (c) Ratio of apoptotic cells determined by using flow cytometry. Cells were stained with propidium iodide and FITC-labeled Annexin V; 20 000 cells were analyzed. Apoptotic cells are distributed in the upper right-hand area. Apoptosis was not observed in cells exposed to supernatant. However, about 9% of cells underwent apoptosis in response to CuO-NPs. Living cells in early apoptotic stage are distributed in the upper left-hand area. Therefore, only 2% of cells were in the early apoptotic stage when cells were exposed to CuO-NPs. (d) Cytotoxicity of CuCl<sub>2</sub> as indicated by the number of viable cells. Arrow indicates concentration of CuCl<sub>2</sub> whose toxicity is similar to that of supernatant. (e) Cytotoxicity of CuCl<sub>2</sub> as indicated by cell viability. Arrow indicates concentration of CuCl<sub>2</sub> whose toxicity is similar to that of supernatant.

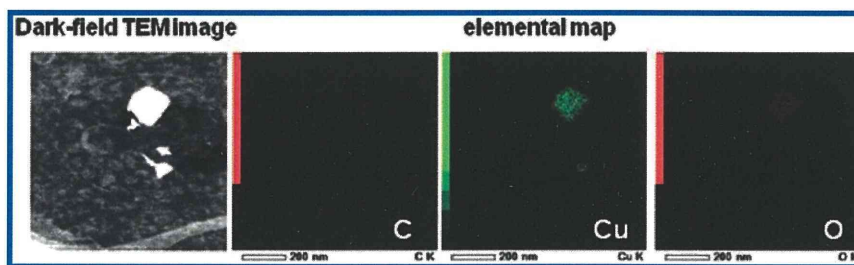


**Figure 3.** Dark-field TEM image and elemental map of NPs inside cells. A549 cells were cultured in medium containing 25  $\mu\text{g}/\text{mL}$  CuO-NPs at 37  $^{\circ}\text{C}$  for 24 h, and then living cells were harvested for the observation. Elemental map suggests the presence of Cu and O.

that affect "nucleobase, nucleoside, nucleotide, and nucleic acid metabolic processes" and "response to stress" and downregulated genes that affect "cell cycle", "mitosis", "cytokinesis", "chromosome segregation", "cellular component organization", and "cellular component morphogenesis" (Figure 4; a list of genes in each category is shown in Supporting Information Tables S1–S6). The

upregulated 31 genes in the response to stress category included genes that encode heat shock proteins (HSPs) (Supporting Information Table S2) and proteins involved in mitogen-activated protein kinase (MAPK) pathways, such as growth arrest and DNA damage-inducible 45  $\beta$  and  $\gamma$  (GADD45B/GADD45G) and nuclear receptors 4A1 and 3 (NR4A1/NR4A3) (Figure 4a and Table 1).

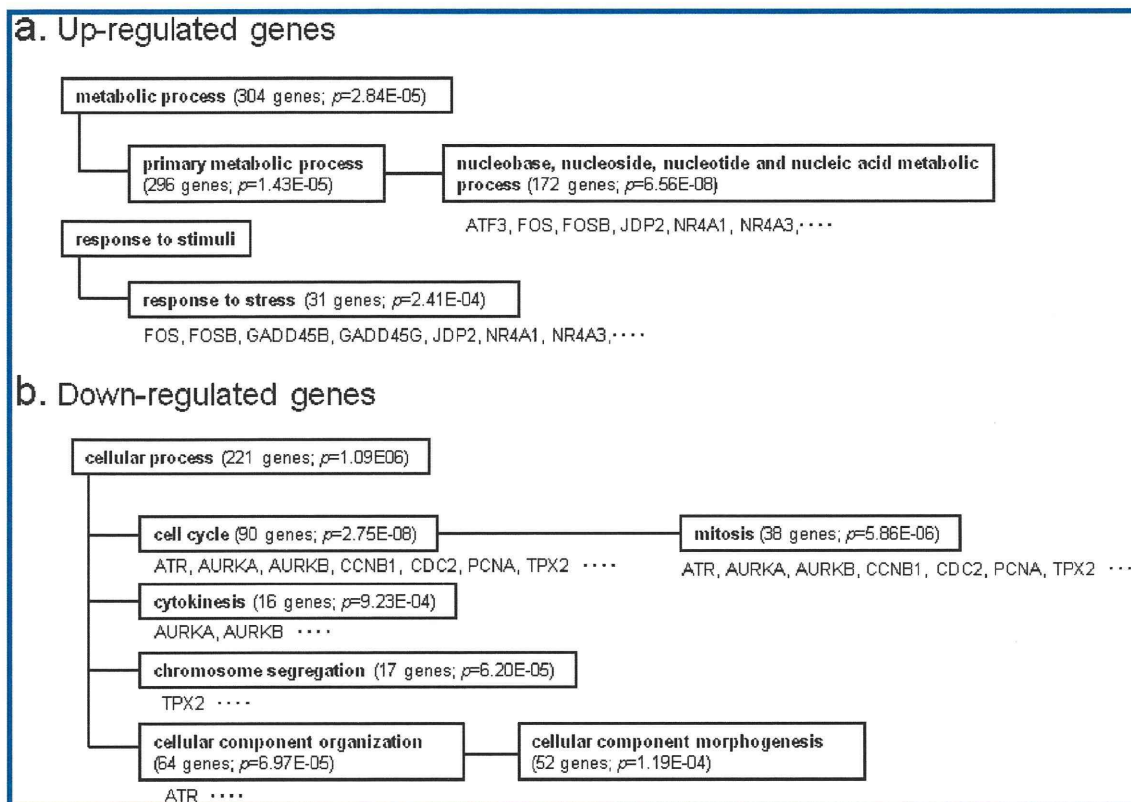


**Figure 4.** Gene ontology classification of genes that were upregulated or downregulated by CuO-NPs. A549 cells were exposed to 25  $\mu\text{g}/\text{mL}$  CuO-NPs for 24 h, and then DNA microarray analysis was used to identify genes that demonstrated a 2-fold or greater change in expression level compared with control cells. These genes were grouped into statistically significant GO functional categories ( $p < 0.001$ ). (a) Functional categories of genes upregulated by CuO-NPs. The numbers within parentheses indicate the number of genes in each category. (b) Functional categories of genes downregulated by CuO-NPs. Representative genes are shown in each category. The gene list for each category is included in Supporting Information (Tables S1–S6).

We confirmed the upregulation of GADD45B/GADD45G and NR4A1/NR4A3 at protein level by using Western blot analysis (Supporting Information Figure S7).

The upregulation of many HSPs suggested that CuO-NPs stimulate protein denaturation. GADD45B and GADD45G are members of the GADD45 family of proteins that are induced by genotoxic stresses and various apoptotic cytokines<sup>11–13</sup> and are involved in cell cycle arrest,<sup>14–19</sup> DNA repair,<sup>20–22</sup> cell survival,<sup>22–27</sup> and apoptosis.<sup>28–37</sup> These functions are mediated by proliferating cell nuclear antigen (PCNA), cell division control 2 (CDC2), cyclin B1 (CCNB1), and cyclin-dependent kinase inhibitor 1A (CDKN1A; also known as p21), which are classified in the GO cell cycle category. PCNA is involved in DNA repair and the transition from the G1 to the S phase of the cell cycle.<sup>20–22</sup> In contrast, CDKN1A inhibits PCNA and blocks the transition from the G1 to the S phase of the cell cycle.<sup>20,38</sup> The CDC2–CCNB1 complex is required for the transition from the G2 to the M phase.<sup>39,40</sup> Although CuO-NPs did not affect the expression of CDKN1A, they downregulated the expression of PCNA, CDC2, and CCNB1 (Figure 4b and Table 1), which suggests that CuO-NPs induce cell cycle arrest in the G1 and G2 phases. In addition, CuO-NPs

downregulated the expression of genes that encode aurora kinase A and B (AURKA/AURKB) and target protein for XKlp2 (TPX2) (Figure 4b and Table 1), which peak during the G2/M transition and are involved in the assembly and maintenance of the spindle.<sup>41</sup>

To confirm that CuO-NPs cause cell cycle arrest, we isolated cells that survived exposure to CuO-NPs and cultured them in fresh culture medium that did not contain CuO-NPs. However, these cells did not proliferate for 72 h (Supporting Information Figure S8a). When we harvested these cells and cultured them again in fresh culture medium that did not include CuO-NPs for an additional 72 h, their proliferative capacity was restored; however, their rate of proliferation lagged behind that of control cells (Supporting Information Figure S8b). These results indicated that the surviving cells were in a state of cell cycle arrest after exposure to CuO-NPs. Since cell cycle arrest is thought to provide time for cells to repair damaged DNA, it is likely that CuO-NPs compromise cell survival.

The expression of GADD45B and GADD45G has been reported to activate the c-Jun N-terminal kinase (JNK) and p38 pathways *via* MAP 3 kinase 1 (MTK1).<sup>28,42,43</sup> In addition, activation of these pathways



TABLE 1. Fold Change of Gene Expression Level Mainly Discussed in This Study

gene name	fold-change ( $\log_2$ ratio) <sup>a</sup>						GO category
	CuO-NP (25 $\mu$ g/mL)		supernatant (contained about 15 $\mu$ g Cu/mL)		CuCl <sub>2</sub> (30 $\mu$ g/mL)	CuCl <sub>2</sub> (60 $\mu$ g/mL)	
	DNA microarray	qPCR	DNA microarray	qPCR	qPCR	qPCR	
GADD4SA	0.24	0.55	-0.76	0.68	0.14	1.07	response to stress
GADD45B	2.96	3.00	-0.02	0.30	-0.42	1.52	response to stress
GADD45G	3.59	3.22	NR	0.61	0.38	1.70	response to stress
PCNA	-1.37	-0.87	NR	-0.28	-0.05	-0.23	cell cycle
CDC2	-1.41	-1.48	-1.16	-1.08	-1.40	-1.22	cell cycle
CCNB1	-1.74	-2.14	-1.33	-1.51	-1.27	-1.46	cell cycle
CDKN1A	0.30	0.78	-0.08	0.63	-0.07	-0.49	cell cycle
FOS	4.48	1.06	NR	-0.14	0.37	0.61	nucleobase, nucleoside, nucleotide and nucleic acid metabolic process; response to stress
FOSB	5.70	3.97	NR	0.68	0.57	3.43	nucleobase, nucleoside, nucleotide and nucleic acid metabolic process; response to stress
ATF3	4.22	1.23	NR	-0.01	0.07	1.14	nucleobase, nucleoside, nucleotide and nucleic acid metabolic process
JDP2	1.13	-0.67	NR	-0.19	-0.36	-0.41	nucleobase, nucleoside, nucleotide and nucleic acid metabolic process
ATR	-1.11	-0.83	-0.20	-0.48	-0.33	-0.51	cell cycle; cellular component organization
TP53	NR	-1.10	NR	-1.12	-0.04	0.15	induction of apoptosis; cell cycle; Nucleobase, nucleoside, nucleotide and nucleic acid metabolic process
NR4A1	5.28	2.82	2.71	1.25	0.89	2.09	nucleobase, nucleoside, nucleotide and nucleic acid metabolic process; response to stress
NR4A2	NR	-1.12	NR	-0.96	0.07	0.33	nucleobase, nucleoside, nucleotide and nucleic acid metabolic process; response to stress
NR4A3	3.06	1.08	NR	0.94	1.55	2.96	nucleobase, nucleoside, nucleotide and nucleic acid metabolic process; response to stress
AURKA	-1.21	-1.62	-0.91	-1.34	-0.59	-1.12	cell cycle; cytokinesis
AURKB	-1.13	-1.76	-0.81	-1.18	-0.96	-1.37	cell cycle; cytokinesis
TPX2	-1.25	-2.13	-1.17	-1.63	-1.16	-2.11	cell cycle; chromosome segregation

<sup>a</sup> Fold-change is represented by logarithmic ratio ( $\log_2$  ratio) to expression level in control. NR: Not reproducible.

induces the activation of the constituent proteins of the activator protein 1 (AP-1) transcription factor complex, such as c-Jun, JunD, and activating transcription factor 2 (ATF2).<sup>44,45</sup> AP-1 is involved in both apoptosis and cell survival.<sup>46,47</sup> To examine how the JNK or p38 pathway is involved in the molecular response to CuO-NP exposure, we treated cells with CuO-NPs and either a JNK interacting protein 1 (JIP-1) peptide or SB239063, which are inhibitors of JNK and p38, respectively. Although the JIP-1 peptide did not have any effect on the number of viable cells, SB239063 markedly reduced the number of viable cells relative to treatment with CuO-NPs alone (Figure 5a and Supporting Information Figure S9). Similar to SB239063, when GADD45B in cells exposed to CuO-NPs was knocked down with small interfering RNA (siRNA) (Supporting Information Figure S10), they were more sensitive to CuO-NPs than cells with normal GADD45B expression, and the number of viable cells decreased (Figure 5b and Supporting Information Figure S11). Together, these results suggest that the upregulation of GADD45B/GADD45G due to CuO-NPs promotes cell survival by activating the p38 pathway. The activation of the p38 pathway in turn activates ATF2, which interacts with FOS, FOSB, and ATF3 in the AP-1

complex. In addition, we observed the upregulation of these proteins by CuO-NPs (Figure 4a and Table 1), which strongly suggested that the underlying mechanism of cell survival involved the p38 pathway.

CuO-NPs also upregulated NR4A1 and NR4A3. These nuclear receptors are involved in both cell survival and apoptosis and are activated *via* the mitogen-activated protein kinase/extracellular signal-regulated kinase 5 (MEK5/ERK5) pathways.<sup>48,49</sup> When NR4A1 in cells exposed to CuO-NPs was knocked down with siRNA (Supporting Information Figure S10), A549 cells were more sensitive to CuO-NPs than cells with normal NR4A1 expression, and the number of viable cells decreased (Figure 5b and Supporting Information Figure S11). These results indicated that the upregulation of NR4A1 is also involved in cell survival after exposure to CuO-NPs.

DNA damage is well-known to activate p53, which induces checkpoint arrest in the G1 and G2/M phases of the cell cycle and apoptosis in cells that cannot recover from DNA damage.<sup>50</sup> The checkpoint function of p53 is activated by the phosphorylation of ataxia telangiectasia mutated (ATM), ataxia telangiectasia and Rad3-related protein (ATR), and checkpoint kinase

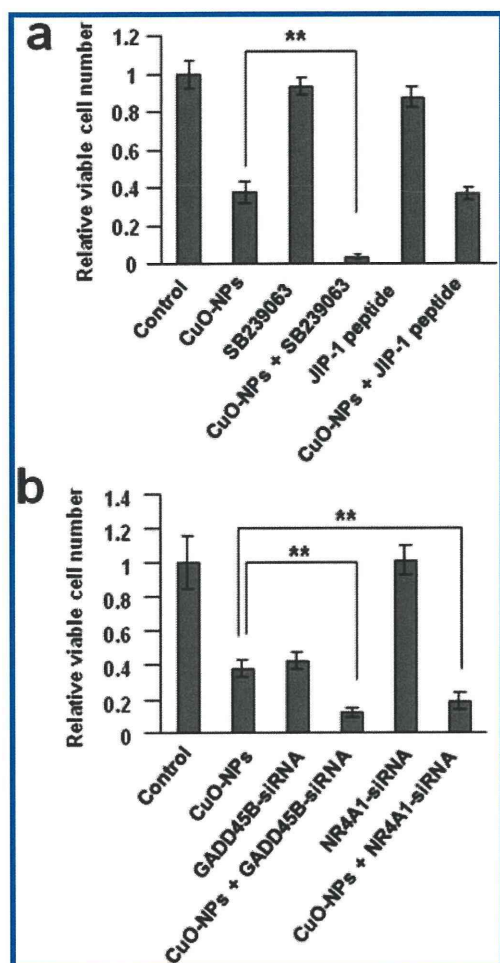


**Figure 5.** Changes in the number of viable cells due to disruption of mitogen-activated protein kinase (MAPK) pathways. After culturing A549 cells for 42 h, p38 or c-Jun N-terminal kinase (JNK) inhibitors or siRNA were added and incubated for 6 h. Subsequently, CuO-NPs were added to a final concentration of 25  $\mu\text{g}/\text{mL}$  and then cultured for 24 h. (a) Effects of SB239063 and JNK interacting protein 1 (JIP-1), which are inhibitors of p38 and JNK, respectively, on the number of viable cells. SB239063 increased the cytotoxicity of CuO-NPs ( $n = 3$ );  $**p < 0.05$ . (b) Effect of siRNA knockdown on the expression of GADD45B and NR4A1 on the cytotoxicity of CuO-NPs. Knockdown of the expression of these genes markedly increased the cytotoxicity of CuO-NPs ( $n = 3$ );  $**p < 0.05$ . The knockdown efficiency for each gene is shown in Supporting Information Figure S10.

1 (Chk1). Subsequently, activated p53 induces the expression of GADD45A and CDKN1A.<sup>30,51–54</sup> Although CuO-NPs downregulated ATR, they did not affect the expression of GADD45A or CDKN1A (Table 1). Therefore, we concluded that p53 does not play a major role in the response of cells exposed to CuO-NPs.

**Contribution of Cu Ions Released from CuO-NPs at the Molecular Level.** In addition to the genes that demonstrated altered expression in response to CuO-NPs, we identified genes that were altered in response to the Cu ions released from CuO-NPs into culture medium to determine their contribution to the molecular response to CuO-NP exposure. Cells exposed to the

supernatant for 24 h upregulated 108 genes (Figure 6a). Of these 108 genes, 54 were also found in the list of 648 genes upregulated by CuO-NPs (Figure 6a and Supporting Information Table S7). Therefore, of 648 genes upregulated by CuO-NPs, 594 upregulated genes were induced by CuO-NPs themselves, but 54 upregulated genes were attributable to Cu ions released from CuO-NPs into the culture medium. After classifying these 54 shared genes into GO functional categories, we did not identify any statistically significantly enriched categories. This finding suggests that released Cu ions do not contribute to changes in cellular functions related to nucleobase, nucleoside, nucleotide, and nucleic acid metabolic processes or response to stress, categories found to be enriched in the classification of genes upregulated by CuO-NPs. The changes in these two functions were specifically induced by CuO-NPs themselves. However, NR4A1 and NR4A3, which are involved in response to stress, were upregulated by both CuO-NPs and the supernatant (Table 1 and Supporting Information Table S7), suggesting that these genes were induced by Cu ions released from the CuO-NPs.

We identified genes encoding super oxide dismutase 2 (SOD2), which functions as a ROS quencher, and 9 genes for metallothionein isomers (MT1A, MT1B, MT1E, MT1F, MT1G, MT1H, MT1L, MT1X, and MT2A) among the 54 common genes upregulated by both CuO-NPs and the supernatant (Figure 6a and Supporting Information Table S7). Since MT isomers help protect cells from oxidative stress due to excess metal ions, such as cadmium, zinc, and copper,<sup>55–58</sup> the released Cu ions may generate ROS. To examine whether CuO-NPs and Cu ions induce ROS in A549 cells, we pretreated cells with *N*-acetylcysteine (NAC), which is a ROS scavenger. NAC protected cells exposed to supernatant from mitochondrial damage (Figure 7a). NAC also partially protected cells exposed to CuO-NPs from mitochondrial damage and cell death (Figure 7b). These findings imply that ROS generation by Cu ions released from CuO-NPs is one of the causes of CuO-NP toxicity.

The supernatant also downregulated 125 genes (Figure 6b). Of these genes, 55 genes were also among the 562 genes downregulated by CuO-NPs (Figure 6b and Supporting Information Table S8). Therefore, of 562 genes downregulated by CuO-NPs, 507 genes were specifically downregulated by CuO-NPs themselves, but 55 genes were downregulated by Cu ions released from CuO-NPs. After classifying these 55 shared downregulated genes into GO categories, we identified statistically significantly enriched functional categories including cell cycle, mitosis, and chromosome segregation (Figure 6c; a list of genes in each category is shown in Supporting Information Table S9). These categories were also identified in the classification of



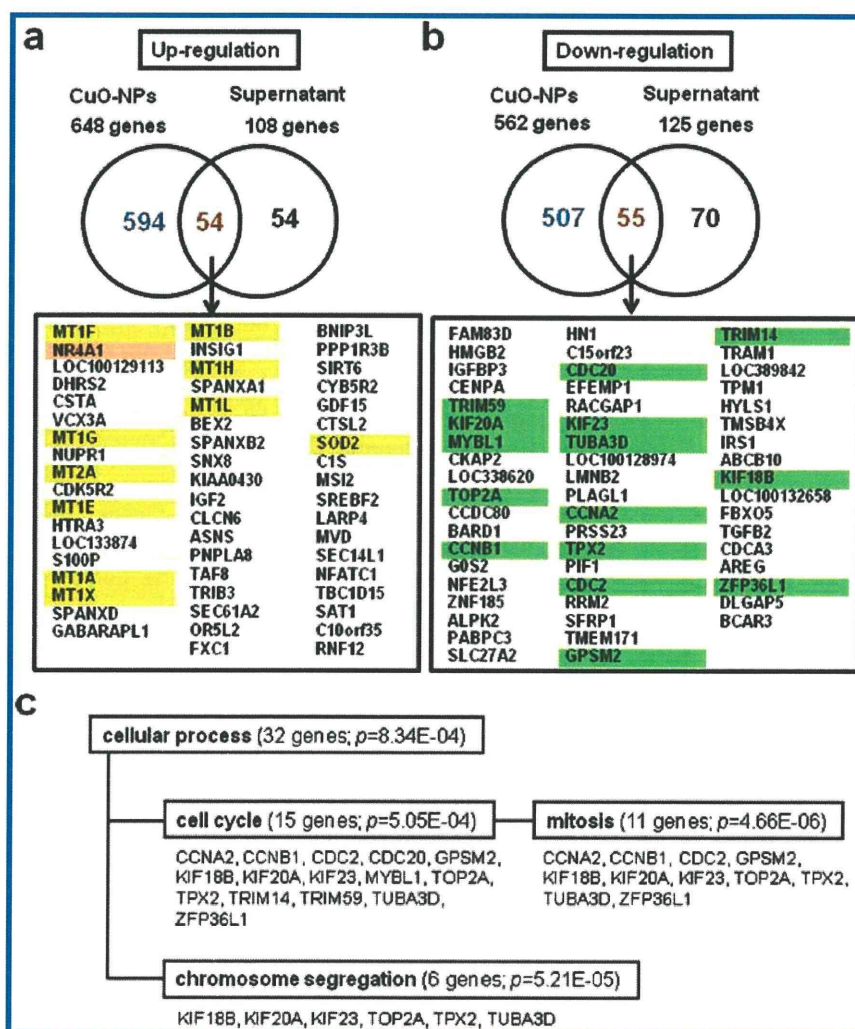


Figure 6. Gene expression altered by both CuO-NPs and released Cu ions. (a) Genes upregulated by both CuO-NPs and supernatant. Of 108 genes that were upregulated in response to supernatant, 54 genes were also upregulated by CuO-NPs. (b) Genes downregulated by both CuO-NPs and supernatant. Of 125 genes that were downregulated in response to supernatant, 55 genes were also downregulated by CuO-NPs. The names of the common genes are boxed. Yellow, orange, and green highlighting of gene names indicate ROS scavenger genes, MAPK-related gene, and cell cycle-related genes, respectively. (c) Gene ontology classification of genes that were downregulated by both CuO-NPs and supernatant. Categories with  $p < 0.001$  were considered statistically significant functional categories. The numbers within parentheses indicate the number of genes in each category. Gene names are listed under each category.

genes downregulated by CuO-NPs (Figure 4b), suggesting that changes in these cellular functions by CuO-NPs were attributable to Cu ions released from CuO-NPs into culture medium.

Among genes downregulated by CuO-NPs, CDC2, CCNB1, PCNA, AURKA/AURKB, and TPX2 were classified into GO categories cell cycle, mitosis, or chromosome segregation (Figure 4b). Downregulation of CDC2, CCNB1, AURKA/AURKB, and TPX2 has been reported to induce cell cycle arrest in the G2 phase,<sup>39–41</sup> and downregulation of PCNA led to cell cycle arrest in the G1 phase.<sup>20,38</sup> Among these genes, CDC2, CCNB1, AURKA/AURKB, and TPX2 were also downregulated by the supernatant, but PCNA was not changed by the supernatant (Table 1). We observed a marked increase in the number of cells in the G2/M phase upon exposure to CuO-NPs and the supernatant

compared with control cells (Figure 8). In addition, an increase in the G1 population accompanied by a decrease in the S phase population was observed in the cells exposed to CuO-NPs compared to the cells exposed to the supernatant (Figure 8). Therefore, released Cu ions are responsible for the cell cycle arrest in the G2 phase induced by CuO-NPs, while cell cycle arrest in the G1 phase is attributable to CuO-NPs themselves. This observation corresponds to the results of gene expression analysis.

A question remains: what causes the toxicity of CuO-NPs themselves? One possibility is the effect of Cu ions released from CuO-NPs taken up into cells. When Cu ions are released from internalized CuO-NPs, the intracellular concentration of Cu ions increases. Indeed, in cells cultured in medium containing 60  $\mu\text{g/mL}$   $\text{CuCl}_2$ , which has a Cu ion concentration twice of that